

Solving Prior Distribution Mismatch in Diffusion Models via Optimal Transport

Zhanpeng Wang¹, Shenghao Li¹, Chen Wang¹, Shuting Cao¹, Na Lei^{1,*}, Zhongxuan Luo¹

¹School of International Information and Software, Ritsumeikan University, Dalian University of Technology

Abstract

In recent years, the knowledge surrounding diffusion models(DMs) has grown significantly, though several theoretical gaps remain. Particularly noteworthy is prior error, defined as the discrepancy between the termination distribution of the forward process and the initial distribution of the reverse process. To address these deficiencies, this paper explores the deeper relationship between optimal transport(OT) theory and DMs with discrete initial distribution. Specifically, we demonstrate that the two stages of DMs fundamentally involve computing time-dependent OT. However, unavoidable prior error result in deviation during the reverse process under quadratic transport cost. By proving that as the diffusion termination time increases, the probability flow exponentially converges to the gradient of the solution to the classical Monge-Ampère equation, we establish a vital link between these fields. Therefore, static OT emerges as the most intrinsic single-step method for bridging this theoretical potential gap. Additionally, we apply these insights to accelerate sampling in both unconditional and conditional generation scenarios. Experimental results across multiple image datasets validate the effectiveness of our approach.

Introduction

In the field of artificial intelligence, the task of generating realistic images using probabilistic models is extremely challenging and has many potential applications in data enhancement(Ruthotto and Haber 2021), image editing, style transfer, etc. Recently, diffusion models(DMs)(Song and Ermon 2019; Ho, Jain, and Abbeel 2020; Song and Ermon 2020; Song et al. 2020) have received much attention for their remarkable achievements in synthesizing audio(Kong et al. 2020; Lee et al. 2021), images generation(Dhariwal and Nichol 2021; Nichol and Dhariwal 2021), and other data modalities(Tashiro et al. 2021; Ho et al. 2022). They go beyond many existing deep generation models, such as generative adversarial networks(GANs)(Goodfellow et al. 2014; Radford, Metz, and Chintala 2015; Arjovsky, Chintala, and Bottou 2017), and variational autoencoders(VAEs)(Kingma and Welling 2013; Rezende, Mohamed, and Wierstra 2014).

DMs include forward process and reverse process. The forward process refers to the add smaller noise gradually

to corrode the original data distribution, which can be understood as a standard diffusion process(Song et al. 2020; Sohl-Dickstein et al. 2015). Subsequently, one can perform reverse inference from noise to image based on the learned *score function*, i.e., the gradient of the logarithmic probability density function(Anderson 1982).

It can be seen from the characteristics of DMs that we usually need to design a reasonable noise scheme in the generative modeling so that the forward process has a unique Gibbs steady state distribution(Gardiner et al. 1985). But it is worth noting that we can only actually terminate diffusion at finite time. Therefore, the noisy data distribution at the end is often not equal to the prior distribution of the sampling process, the existence of *prior error* leads to theoretically we cannot get the desired goal even if the score match exactly. Although in (Khrukov et al. 2022; Franzese et al. 2023), authors all show that as diffusion duration increases, the prior error will converges exponentially to zero. However, this also means that more computing resources are required(Lyu et al. 2022).

To eliminate prior error without increasing the calculation cost, it is intuitive to use single step generator to construct probability transformation from the prior distribution of the reverse process to the posterior distribution of the forward process, such as GANs(Lyu et al. 2022; Zheng et al. 2022), VAEs(Lyu et al. 2022), conditional transport(CT)(Zheng et al. 2022) and optimal transport(OT)(Li et al. 2023). While these models are empirical and no more detailed theoretical explanations are provided for elimination of prior error. Therefore, a natural question is troubling us—*which generator is the best used to eliminate prior error in DMs?*

If the economic issue of transport cost is under consideration, the OT map should be the focal point due to its geodesic properties within the probability space(Villani et al. 2009). But the straightforward decision is not based on the deeper connection between DMs and OT theory, so it is a little "blunt". Up to now, there have been many researches involving this link. In (Kwon, Fan, and Lee 2022), the authors show that the matching loss of DMs can constrain the Wasserstein metric. Khrukov et al.(Khrukov et al. 2022) and Lavenant et al.(Lavenant and Santambrogio 2022) give simple positive and negative examples respectively to investigate whether the diffusion process can be regarded as geodesic. Whereafter, the latest work (Zhang et al. 2024a)

*corresponding author, nalei@dlut.edu.cn

generalizes their conclusions and shows that the continuous probability flow coincides with OT map under certain conditions. These works all point to that there exist some consistency between DMs and OT.

Inspired by previous works, this paper further explores the intrinsic relationship between probability flow and OT theory, and answers mathematically the question above: **Optimal transport provides the most intrinsic prior error eliminator for diffusion models**. Our main contributions and findings are summarized as follows:

- We show that the diffusion model is a two-stage time-dependent optimal transport calculation method. The error between the learned reverse transport map and the ground truth is bounded by the root of score matching loss (8).

- Theoretically, we analyze that the ineliminable prior error in classical diffusion models will lead to a potential gap. Even if the score is accurately learned, the deterministic sampling locus still not be a geodesic.

- We prove that the probability flow can converge exponentially to the gradient of the solution to the Monge-Ampère equation. Therefore, we recommend that the termination part of the diffusion framework be replaced by the static optimal transport, which can completely eliminate the prior error without increasing the computational cost.

- Our viewpoint can be naturally extended to sampling acceleration for unconditional and conditional generation. More importantly, experimental results obtained from various image datasets corroborate our conclusions.

Notations \mathbf{x} represents the state variable in n -dimensional Euclidean space \mathbb{R}^n and t is for time; d and ∂ imply differential and partial differential operators, respectively; ∇ and $\nabla \cdot$ mean the gradient and the divergence operators, respectively; $\|\cdot\|_2$ and $\|\cdot\|_\infty$ provide the 2-norm of a vector or matrix and ∞ -norm of a scalar function, respectively; $\mathbb{R}_{\geq 0}$ and $\mathbb{R}_{> 0}$ signify the set of non-negative and positive real numbers, respectively; \circ shows the composition of multiple function maps; $|\cdot|$ denotes the cardinality of set; $\#$ indicates push-forward of probability density; $\mathcal{W}_2(\cdot, \cdot)$ represents the Wasserstein distance between two probability densities; $sum(\cdot)$ shows the sum of all the elements of a vector.

Preliminaries and related works

Optimal transport theory

In this section, we introduce the concise description of the static/dynamic OT problem with quadratic cost $c(\mathbf{x}, \mathbf{y}) = \frac{1}{2}\|\mathbf{x} - \mathbf{y}\|_2^2$ in turn and illustrate their compatibility.

Static optimal transport Assuming that ρ_0 and $\rho_1 \in \mathcal{P}(\mathbb{R}^n, \mathcal{W}_2)$ represent two continuous probability density functions, we call a map $M : \mathbb{R}^n \rightarrow \mathbb{R}^n$ measure-preserving $M_{\#}\rho_0 = \rho_1$, if $\int_B \rho_1(\mathbf{y}) d\mathbf{y} = \int_{M^{-1}(B)} \rho_0(\mathbf{x}) d\mathbf{x}$ holds for any Borel set $B \subset \mathbb{R}^n$. The Monge problem(Monge 1781) aims to find the OT map M_{ot} among all measure-preserving maps, that is

$$M_{ot} = \arg \inf_{M_{\#}\rho_0 = \rho_1} \frac{1}{2} \int_{\mathbb{R}^n} \|\mathbf{x} - M(\mathbf{x})\|_2^2 \rho_0(\mathbf{x}) d\mathbf{x}, \quad (1)$$

the one that minimizes the total transport cost. Moreover, there exists a convex function $u(\mathbf{x}) : \mathbb{R}^n \rightarrow \mathbb{R}$ (also known

as the *Brenier potential*(Brenier 1991)) that satisfies that $\nabla u = M_{ot}$ is the unique solution to (1) when quadratic cost. From Jacobian equation, one can get the necessary condition for Brenier potential, namely, Monge-Ampère equation(Villani et al. 2009)

$$\det \nabla^2 u(\mathbf{x}) = \frac{\rho_0(\mathbf{x})}{\rho_1 \circ \nabla u(\mathbf{x})}. \quad (2)$$

Dynamic optimal transport Benamou and Brenier introduce an alternative analytical framework by connecting (1) to continuum mechanic frameworks(Benamou and Brenier 2000). They investigate the time-dependent transport through the dynamic evolution from ρ_0 at initial time $t = 0$ to ρ_1 at end time $t = 1$ and denote the intermediate process as $\rho_t, t \in [0, 1]$, which satisfies the continuity equation

$$\frac{\partial \rho_t(\mathbf{x})}{\partial t} + \nabla \cdot (\mathbf{v}(\mathbf{x}, t) \rho_t(\mathbf{x})) = 0, \quad (3)$$

where $\mathbf{v}(\mathbf{x}, t) : \mathbb{R}^n \times [0, 1] \rightarrow \mathbb{R}^n$ represents the time-dependent velocity field that describes the dynamic transport process. Therefore, Benamou-Brenier formulation aims to find the velocity field with minimum total kinetic energy under the premise of satisfying the boundary conditions ρ_0, ρ_1 and conservation of mass formula (3), that is,

$$\mathbf{v}_{ot}(\mathbf{x}, t) = \arg \inf_{\mathbf{v}} \frac{1}{2} \int_0^1 \mathbb{E}_{\rho_t} [\|\mathbf{v}(\mathbf{x}, t)\|_2^2] dt. \quad (4)$$

Compatibility The static Monge problem (1) and the dynamic Benamou-Brenier problem (4) are equivalent and compatible in terms of the quadratic transport cost(Villani et al. 2009). Specifically, when the boundary conditions are the same, the total transport cost of the OT map M_{ot} is equal to the total kinetic energy of the optimal velocity field \mathbf{v}_{ot} , so they are both taken as \mathcal{W}_2 metrics. In addition, the two can also be transformed by McCann displacement interpolation(McCann 1997).

Diffusion models and probability flow

The intrinsic driver of DMs is stochastic differential equation(SDE), which is usually expressed as

$$d\mathbf{x} = -f(t) \mathbf{x} dt + g(t) d\mathbf{W}_t, \mathbf{x}(0) \sim p_0(\mathbf{x}), \quad (5)$$

where $f(t) : [0, T] \rightarrow \mathbb{R}_{\geq 0}$ represents the non-negative drift coefficient, $g(t) : [0, T] \rightarrow \mathbb{R}_{> 0}$ implies the positive diffusion term, p_0 is the initial data distribution and \mathbf{W}_t stands for a time-dependent n -dimensional standard Wiener process. The marginal distribution p_t of the solution to (5) at time t is strictly described by the Fokker-Planck equation(FPE)(Risken and Risken 1996)

$$\frac{\partial p_t(\mathbf{x})}{\partial t} + \nabla \cdot (-f(t) \mathbf{x} p_t(\mathbf{x})) - \frac{g(t)^2}{2} \Delta p_t(\mathbf{x}) = 0, \quad (6)$$

and has a unique steady state Gibbs distribution(Gardiner et al. 1985), which we refer to as p_∞ . According to (6), there exists a deterministic process, which we call the probability flow ordinary differential equation(ODE)(Song et al. 2020)

$$\frac{d\mathbf{x}}{dt} = -f(t) \mathbf{x} - \frac{g(t)^2}{2} \nabla \log p_t(\mathbf{x}), \mathbf{x}(0) \sim p_0(\mathbf{x}) \quad (7)$$

that shares the same marginal probability density p_t with (5). The training process of DMs refers to use a parameterized

neural network $\mathbf{S}_\theta(\mathbf{x}, t)$ to approach score $\nabla \log p_t(\mathbf{x})$, and the target loss function $\mathcal{J}_{SM}(\theta, \phi, 0, T)$ is defined as the weighted mean square error(MSE)(Song et al. 2020)

$$\frac{1}{2} \int_0^T \phi(t) \mathbb{E}_{p_t} [\|\mathbf{S}_\theta(\mathbf{x}, t) - \nabla \log p_t(\mathbf{x})\|_2^2] dt, \quad (8)$$

where θ is a learnable parameter and $\phi(t) : [0, T] \rightarrow \mathbb{R}_{>0}$ means a positive weight associated with time t . In practice, however, \mathcal{J}_{SM} is often difficult to quantify due to lack of information about $\nabla \log p_t(\mathbf{x})$ (Song et al. 2021). Therefore, it is common to convert it to a treatable conditional score matching loss $\mathcal{J}_{DSM}(\theta, \phi, 0, T)$ (Vincent 2011) via letting $p_t(\mathbf{x}) = p_t(\mathbf{x}(0)) p_{0t}(\mathbf{x}|\mathbf{x}(0))$, here p_{0t} indicates the probabilistic transition kernel from time 0 to t .

Related works

Relationship between DMs and OT theory The authors of (Khrukov et al. 2022) show that the probability flow can be considered as an OT map under the initial assumption of a multivariate normal distribution. However, a counterexample of continuous initial distribution is provided in (Lavenant and Santambrogio 2022) to show that the probability flow is not optimal. Recently, Zhang et al.(Zhang et al. 2024a) further extend their conclusion and argue that the probability flow over any closed interval in $(0, \infty)$ coincides with the OT map under the condition of finite training samples. In addition, Kwon et al.(Kwon, Fan, and Lee 2022) indicate that DMs also minimize the Wasserstein distance between the true distribution and the generated distribution.

Singularity of DMs Under the initial condition of discrete probability density, the score $\nabla \log p_t(\mathbf{x})$ does not exist at $t = 0$, resulting in $\mathbf{S}_\theta(\mathbf{x}, t)$ cannot be Lipschitz continuous across $[0, T]$ (Zhang et al. 2024b). Therefore, Song et al.(Song et al. 2020) suggest to choose a small $\varepsilon > 0$ to terminate the sampling process to ensure the quality of the generated image(Lu et al. 2022; Song et al. 2023; Zhang et al. 2024b). In addition, there are numerous theoretical analysis based on this idea(Benton et al. 2023; Li, Chen, and Li 2024).

Main results

In this section, we will elaborate the main theoretical results of this paper. For a more detailed analysis and proof, refer to section C of the Appendix.

Diffusion models secretly compute the dynamic optimal transport

Under the initial condition of discrete probability density $p_0(\mathbf{x}) = \frac{1}{|\mathcal{I}|} \sum_{i \in \mathcal{I}} \delta(\mathbf{x} - \mathbf{x}_0^i)$, $|\mathcal{I}| < \infty$, Zhang et al.(Zhang et al. 2024a) prove that the probability flow, the analytical solution of (7), conform to dynamic OT map on any closed time interval in $(0, \infty)$. Therefore, $\mathbf{v}_{ot}(\mathbf{x}, t) = -f(t)\mathbf{x} - \frac{g(t)^2}{2} \nabla \log p_t(\mathbf{x})$ is the corresponding optimal velocity field with the lowest kinetic energy under the \mathcal{W}_2 metric, and then we express the probability flow from time s to t as $M_{ot}^{s,t} : \mathbb{R}^n \rightarrow \mathbb{R}^n$, $M_{ot}^{s,t}(\mathbf{x}_s) = \mathbf{x}_t$, here $0 < s, t < \infty$. It is worth noting that the probability flow is reversible(Lavenant and Santambrogio 2022), and $(M_{ot}^{s,t})^{-1} = M_{ot}^{t,s}$. In this

view, the training and sampling processes of DMs are equivalent to different steps in calculating time-dependent OT.

(I) Training stage: Matching the optimal velocity field. If only optimization results are considered, then the weighted MSE loss function (8) over $[\varepsilon, T]$ is equal to

$$\int_\varepsilon^T \phi(t) \mathbb{E}_{p_t} [\|\mathbf{v}_\theta(\mathbf{x}, t) - \mathbf{v}_{ot}(\mathbf{x}, t)\|_2^2] dt, \quad (9)$$

where $\mathbf{v}_\theta(\mathbf{x}, t) = -f(t)\mathbf{x} - \frac{g(t)^2}{2} \mathbf{S}_\theta(\mathbf{x}, t)$.

(II) Sampling stage: Solving the probability flow ODE. Substituting the learned $\mathbf{v}_\theta(\mathbf{x}, t)$ into (7) gives an approximation reverse probability flow ODE

$$d\mathbf{x} = \mathbf{v}_\theta(\mathbf{x}, t) dt, t \in [\varepsilon, T], \mathbf{x}(T) \sim q_T(\mathbf{x}), \quad (10)$$

which is also the locus equation of the sampling process with q_T as the initial prior noise distribution. The solution of (10) provides an approximation $M_{ot}^{T,\varepsilon} : \mathbb{R}^n \rightarrow \mathbb{R}^n$ of the time-dependent OT map $M_{ot}^{T,\varepsilon}$.

Theorem 1 Assume that $M_{ot}^{T,\varepsilon}$ and $M_\theta^{T,\varepsilon}$ are the true solution of reverse probability flow ODE (7) and (10), respectively, with $q_T = p_T$ as the same initial condition, then

$$\|M_{ot}^{T,\varepsilon} - M_\theta^{T,\varepsilon}\|_{L_2(q_T)} \leq \sqrt{\frac{T-\varepsilon}{2I(\varepsilon)^2}} \mathcal{J}_{SM}(\theta, \phi, \varepsilon, T)^{\frac{1}{2}}, \quad (11)$$

here $I(t) = \exp\left(\int_0^t (f(\tau) + \frac{g(\tau)^2}{2} L_{\mathbf{S}_\theta}(\tau)) d\tau\right)$ stands for integrating factor, $\phi(t) = g(t)^4 I(t)^2$, and $L_{\mathbf{S}_\theta}$ implies the continuous Lipschitz constant of $\mathbf{S}_\theta(\mathbf{x}, t)$ over $[\varepsilon, T]$.

Corollary 1 Under the same setting as in Theorem 1. If p_{0t} satisfies $\text{Var}[\mathbb{E}[(\nabla \log p_{0t}(\mathbf{x}|\mathbf{x}_0))^T | \mathbf{x}_0]] = 0$, then we have

$$\|M_{ot}^{T,\varepsilon} - M_\theta^{T,\varepsilon}\|_{L_2(q_T)} \leq \sqrt{\frac{T-\varepsilon}{2I(\varepsilon)^2}} \mathcal{J}_{DSM}(\theta, \phi, \varepsilon, T)^{\frac{1}{2}}. \quad (12)$$

Corollary 2 Under the same setting as in Corollary 1. Let $q_\varepsilon = (M_\theta^{T,\varepsilon})_{\#} q_T$, if $\mathbf{v}_\theta(\mathbf{x}, t)$ solves problem (4) with two boundary conditions $\rho_0 = q_T$ and $\rho_1 = q_\varepsilon$, then we have

$$\mathcal{W}_2(p_\varepsilon, q_\varepsilon) \leq \sqrt{\frac{T-\varepsilon}{2I(\varepsilon)^2}} \mathcal{J}_{DSM}(\theta, \phi, \varepsilon, T)^{\frac{1}{2}}. \quad (13)$$

Remark 1 As can be seen from Theorem 1 and Corollary 1, the optimization of DMs also secretly makes the parameterized transport map close to the optimal ground truth.

Remark 2 We need to point out that Denoising Diffusion Probabilistic Models(DDPM)(Ho, Jain, and Abbeel 2020) satisfy variance condition in Corollary 1 refer to (Kwon, Fan, and Lee 2022).

The potential gap prevents the reverse process from optimality

It is worth noting that in practice we take the simple Gibbs distribution p_∞ instead of p_T as the vanilla distribution q_T of the reverse process(Ho, Jain, and Abbeel 2020; Song et al. 2020), namely $q_T = p_\infty$, so there exist a prior error $\mathcal{W}_2(p_T, q_T) \neq 0$, which leads to an insurmountable gap between $M_\theta^{T,\varepsilon}$ and $M_{ot}^{T,\varepsilon}$. We still have $\mathcal{W}_2(p_\varepsilon, q_\varepsilon) \neq 0$ in the light of Theorem 2 even if $\mathbf{S}_\theta(\mathbf{x}, t)$ reaches precisely the optimal target $\nabla \log p_t(\mathbf{x})$ on $\mathbb{R}^n \times [\varepsilon, T]$. In other words, the irreducibility of the potential gap makes the sampling process not optimal in any way.

Theorem 2 If $q_T = p_\infty$, $\mathbf{S}_\theta(\mathbf{x}, t) \equiv \nabla \log p_t(\mathbf{x})$ on $\mathbb{R}^n \times [\varepsilon, T]$, we denote $q_\varepsilon = (M_\theta^{T,\varepsilon})_\# q_T$, then $\mathcal{W}_2(p_\varepsilon, q_\varepsilon)$ can be estimated as follows

$$\frac{\bar{I}(T)}{\bar{I}(\varepsilon)} \mathcal{W}_2(p_T, q_T) \leq \mathcal{W}_2(p_\varepsilon, q_\varepsilon) \leq \frac{I(T)}{I(\varepsilon)} \mathcal{W}_2(p_T, q_T), \quad (14)$$

where $\bar{I}(t) = \exp\left(\frac{1}{2} \int_0^t f(\tau) d\tau\right)$.

Remark 3 The Theorem 2 means that the reverse process obtained by optimizing the loss function (8) must have deviation as long as $\mathcal{W}_2(p_T, q_T) \neq 0$.

Optimal transport is the most intrinsic prior error eliminator

Based on the contraction property of the Wasserstein distance (Carrillo, McCann, and Villani 2006; Kwon, Fan, and Lee 2022), one can exponentially mitigate the effect of the prior error by prolonging the diffusion time T , which dramatically increases the computing cost. In order to escape this contradictory dilemma, we consider the compatibility between the OT problem (1) and (4). In particular, we use $\nabla u_{T'}^{\rightarrow}$ as a static OT map from p_T to p_∞ , which obviously cannot be regarded as the probability flow defined on finite interval $[T, s]$, here $s > T$. However, Theorem 3 gives an upper bound of the difference between them and Remark 4 states that the dissimilarity will exponentially approach to zero as s increases. Besides that, it also recommends that $\nabla u_{T'}^{\rightarrow}$ be the generalized probability flow over $[T, \infty)$.

Theorem 3 Suppose $u_{T'}^{\rightarrow}$ implies the analytical solution of the Monge-Ampère equation (2) with boundary condition $\rho_0 = p_T$ and $\rho_1 = p_\infty$, then there exists a constant K independent of s that satisfies

$$\|\nabla u_{T'}^{\rightarrow} - M_{ot}^{T,s}\|_{L_2(p_T)} \leq K \left\{ \frac{\bar{I}(s)}{\bar{I}(T)} \mathcal{W}_2(p_\infty, p_T) \right\}^{\frac{2}{15}}. \quad (15)$$

Remark 4 Since $f(t)$ makes $\lim_{s \rightarrow \infty} \int_T^s f(t) dt = \infty$ hold, we have $\lim_{s \rightarrow \infty} \bar{I}(s) = 0$ in Theorem 3.

Remark 5 Similarly, there exists a unique Brenier potential $u_{T'}^{\leftarrow}$, which satisfies $\nabla u_{T'}^{\leftarrow} = (\nabla u_{T'}^{\rightarrow})^{-1}$ and the Monge-Ampère equation (2) with boundary constraints with boundary condition $\rho_0 = p_\infty$ and $\rho_1 = p_T$.

The above analysis reveals that static OT is the best single-step prior error eliminator, providing not only the most economical transport cost but also intrinsic compatibility with probability flow. Specifically, we leave the forward process unchanged, and instead treat $q_T = \nabla u_{T'}^{\leftarrow}(p_\infty)$ as the initial distribution of the sampling process. Corresponding error analysis is shown in Theorem 4 and Corollary 3.

Extended discussion

In this section, we will show that our approach can be extended to sampling acceleration in unconditional and conditional generation. It is worth mentioning that a more detailed algorithm flow is shown in section D of the Appendix. Subsequently, we will verify each of them in the experimental section.

(I) OT accelerated sampler. Based on the previous analysis of Theorem 3, we know that static OT provides the most intrinsic accelerated sampler for DMs. Therefore, we choose a smaller time $\varepsilon < T' \ll T$ to terminate the diffusion, and then replace the remaining complicated two-stage calculation of time-dependent OT in DMs with solving the Monge-Ampère equation (2), where $\rho_0 = p_\infty$ and $\rho_1 = p_{T'}$. Assuming that the parameterized Brenier potential energy we learn is $u_{\theta'}^{\leftarrow}$, then our accelerated generation distribution can be concretized as $q_\varepsilon = M_{\theta'}^{T',\varepsilon} \circ \nabla u_{\theta'}^{\leftarrow}(p_\infty)$.

(II) Geometric view for solving the Monge-Ampère equation. The geometric variational method, which was established by (Gu et al. 2016) and was widely applied in deep learning through convex optimization (Lei et al. 2019; An et al. 2020), reveals the intrinsic connection between Brenier (Brenier 1991) and Alexandrov theory (Alexandrov 2005). We briefly describe it from the discrete perspective, and when the number of samples is large enough, it can be generalized to the continuous case.

Given discrete data set $\mathcal{X}_{T'} = \{\mathbf{x}_{T'}^i\}_{i \in \mathcal{I}} \stackrel{i.i.d.}{\sim} p_{T'}$, the target Dirac probability density $p_{\mathcal{X}_{T'}} = \frac{1}{|\mathcal{I}|} \sum_{i \in \mathcal{I}} \delta(\mathbf{x} - \mathbf{x}_{T'}^i)$. Then the static OT map $\nabla u_{\theta'}^{\leftarrow} : (\Omega, p_\infty) \rightarrow (\mathcal{X}_{T'}, p_{\mathcal{X}_{T'}})$ induces the cell decomposition in the source domain Ω , namely, $\Omega = \bigcup_{i \in \mathcal{I}} W_{T'}^i$, which satisfies $\nabla u_{\theta'}^{\leftarrow}(W_{T'}^i) = \mathbf{x}_{T'}^i$ and $\int_{W_{T'}^i} p_\infty(\mathbf{z}) d\mathbf{z} = \frac{1}{|\mathcal{I}|}$. We construct triangulation \mathcal{T}

based on $\{\mathbf{c}_{T'}^i\}_{i \in \mathcal{I}}$ to reflect the adjacency of the cell cavity, where $\mathbf{c}_{T'}^i = \int_{W_{T'}^i} \mathbf{z} p_\infty(\mathbf{z}) d\mathbf{z}$ means the center of gravity of cell $W_{T'}^i$. However, there exist some polyhedrons that transverse the singular set when the support of the data distribution is non-convex (Figalli 2010; Chen and Figalli 2017), which means that different vertices of the polyhedron belongs to different mode. Specifically, we can detect if edge $[\mathbf{c}_{T'}^i, \mathbf{c}_{T'}^j]$ crosses the singular set (Luo et al. 2022)

by checking the angles $\arccos \frac{\langle \mathbf{x}_{T'}^i, \mathbf{x}_{T'}^j \rangle}{\|\mathbf{x}_{T'}^i\|_2 \|\mathbf{x}_{T'}^j\|_2}$ like (An et al. 2020). Eventually, we discard these edges that span singular sets and the remainder of \mathcal{T} is written as $\widehat{\mathcal{T}}$, which can be decomposed into different simple connected branches $\widehat{\mathcal{T}} = \bigcup_{k \in \mathcal{K}} \widehat{\mathcal{T}}_k$, where \mathcal{K} implies a categories set, $\widehat{\mathcal{T}}_k$ stands for complex and $\widehat{\mathcal{T}}_k \cap \widehat{\mathcal{T}}_{k'} = \emptyset$ for $\forall k \neq k'$.

Unconditional generation. Sampling latent code $\mathbf{z} \sim p_\infty$, if $\mathbf{z} \in \widehat{\mathcal{T}}$, we can find the n -dimensional simplex σ that contains \mathbf{z} . Let the matrix of all vertices of σ be represented by $\mathbf{C}_\sigma \in \mathbb{R}^{n \times (n+1)}$, therefore there exists unique positive weight vector $\boldsymbol{\lambda} \in \mathbb{R}^{n+1}$ that satisfies $\mathbf{z} = \mathbf{C}_\sigma \boldsymbol{\lambda}$ and $\text{sum}(\boldsymbol{\lambda}) = 1$. Then $\mathbf{x}_{T'} = \nabla u_{\theta'}^{\leftarrow}(\mathbf{C}_\sigma) \boldsymbol{\lambda}$. The whole process above is summarized in schematic Fig. 2 and Algorithm 1 in the Appendix.

Conditional generation. Assume that the noisy data set $\mathcal{X}_{T'}$ has a corresponding label $L = \{l_i\}_{i \in \mathcal{I}}, l_i \in \mathcal{K}$ and $\mathcal{C}(\mathbf{x}) : \mathcal{X}_{T'} \rightarrow \mathcal{K}$ means classification map. Then we have $\mathcal{C} \circ \nabla u_{\theta'}^{\leftarrow}(\mathbf{c}_{T'}^i) = l_i$ and $\mathcal{C} \circ \nabla u_{\theta'}^{\leftarrow}(\mathbf{c}_{T'}^j) = \mathcal{C} \circ \nabla u_{\theta'}^{\leftarrow}(\mathbf{c}_{T'}^i)$ for any $\mathbf{c}_{T'}^i, \mathbf{c}_{T'}^j \in \widehat{\mathcal{T}}_k, k \in \mathcal{K}$. If one want to generate a new sample labeled $l_{new} \in \mathcal{K}$, he or she just need to randomly sample \mathbf{z} the complex region $\widehat{\mathcal{T}}_k$ with the known label l_{new} ,

namely $z \in \widehat{\mathcal{T}}_k$ and $\mathcal{C} \circ \nabla u_{\theta'}^{\leftarrow}(\widehat{\mathcal{T}}_k) = l_{new}$. Specifically, we start by randomly uniformly selecting a n -dimension simplex in $\widehat{\mathcal{T}}_k$, denoted as σ , whose vertex matrix is represented by $C_\sigma \in \mathbb{R}^{n \times (n+1)}$. Then the vector β is extracted from $n+1$ -dimensional uniform distribution to construct the weight $\lambda = \beta / \text{sum}(\beta)$. Then the sampling point in the complex $\widehat{\mathcal{T}}_k$ is $z = C_\sigma \lambda$, so the final new sample generated by linear expansion is $x_{T'} = \nabla u_{\theta'}^{\leftarrow}(C_\sigma) \lambda$. The Fig. 3 and Algorithm 2 in the attachment record the entire process.

(III) Error analysis. Let the analytical Brenier potential satisfies the Monge-Ampère equation (2) with boundary constraint $\rho_0 = p_\infty$ and $\rho_1 = p_{T'}$ as $u_{T'}^{\leftarrow}$, and the geometric variational guides us to approximate it by θ' -parameterized convex continuous network $u_{\theta'}^{\leftarrow}$. Therefore we have a substitute $\nabla u_{\theta'}^{\leftarrow}$ for the true OT map $\nabla u_{T'}^{\leftarrow}$, and Theorem 4 measures the upper bound of the error between them.

Theorem 4 *Suppose $u_{\theta'}^{\leftarrow}$ is an approximation of true Brenier potential energy $u_{T'}^{\leftarrow}$, then we have*

$$\|\nabla u_{T'}^{\leftarrow} - \nabla u_{\theta'}^{\leftarrow}\|_{L_2(p_\infty)} \leq K \|u_{T'}^{\leftarrow} - u_{\theta'}^{\leftarrow}\|_\infty^{\frac{1}{2}}, \quad (16)$$

where K is a positive constant that only relates to Ω and $\mathcal{X}_{T'}$.

Corollary 3 *The error upper bound of the generation distribution of DMs with OT prior eliminator is*

$$\begin{aligned} \mathcal{W}_2(p_\varepsilon, q_\varepsilon) &\leq \sqrt{2(T' - \varepsilon)} \mathcal{J}_{SM}(\theta, \phi, \varepsilon, T')^{\frac{1}{2}} \\ &+ K \frac{I(T')}{I(\varepsilon)} \|u_{T'}^{\leftarrow} - u_{\theta'}^{\leftarrow}\|_\infty^{\frac{1}{2}}. \end{aligned} \quad (17)$$

(IV) Relationship with ODE accelerated sampling of DMs. In order to speed up the inference process of images, this kind of method aims to explore the higher-order numerical solution of probability flow ODE (10) with initial condition $q_T = p_\infty$. Existing accelerated solver of probability flow ODE include DPM-Solver(Lu et al. 2022), diffusion exponential integrator sampler(DEIS)(Zhang and Chen 2022), predictive correction framework(UniPC)(Zhao et al. 2024), and so on. They usually ignore the impact of prior error, and the numerical errors will gradually accumulate due to long-term diffusion. By proving that the probability flow converges to the gradient of solution to the Monge-Ampère equation(see Theorem 3), we give a more analytical single step ODE accelerated sampler, which eliminates the prior error. More importantly, our approach only needs to train DMs over time interval $[\varepsilon, T']$, thus reducing training cost, which is not covered by other above-mentioned existing ODE acceleration methods.

(V) Relationship with early stop strategy of DMs. This is a more direct acceleration strategy designed to replace most diffusion steps with single step probability distribution transformation, such as GANs & CT(Zheng et al. 2022), GANs & VAEs(Lyu et al. 2022), etc. Therefore the early stop strategy is only a special case of the prior error problem. Moreover, we show that OT is the eliminator that best fits DMs, which provides deeper insight into (Li et al. 2023)'s framework. This dropout idea is extended by (Chung, Sim, and Ye 2022) to super-resolution, image inpainting and MRI reconstruction task. It is worth mentioning that both (Li et al.

2023) and (Franzese et al. 2023) try to find the optimal number of diffusion steps by experiment, but the emphasis is different.

Experiments

In this section, we will present extended visualizations of OT as a prior error eliminator for accelerating sampling in unconditional and condition generation. All experiments were conducted by training the model on two RTX 3090 GPUs and performing sampling on a single NVIDIA A40. More detailed experimental parameters and visual results are shown in section E of the Appendix.

Experiment settings

Datasets. In this paper, we perform the proposed approach mainly on three public datasets, consisting of Cifar-10 32×32 (Krizhevsky, Hinton et al. 2009), CelebA 64×64 (Liu et al. 2015) and FFHQ 256×256 (Russakovsky et al. 2015).

Baseline methods. Comparison models can be divided into two classes, the first is ODE or truncated acceleration strategies that are extremely relevant to our model, including DPM-Solver(Lu et al. 2022), DEIS(Zhang and Chen 2022), UciPC(Zhao et al. 2024), ES-DDPM(Lyu et al. 2022) and TDPM & TDPM+(Zheng et al. 2022). The other part is the classical diffusion modeling method used to compare the generating effect, including DDIM(Song, Meng, and Ermon 2020), NCSNv2(Song and Ermon 2020) and EDM(Karras et al. 2022).

Evaluation metrics. We consider diffusion Terminate Time T , Sampling Time and number of function evaluations(NFE) as criteria for modeling efficiency, whereas Prior Error $\mathcal{W}_2(p_T, q_T)$ is taken to mean the effects of various eliminators. In addition, Fréchet Inception Distance(FID)(Heusel et al. 2017) represents the quality of the generated image, while Precision & Recall in (Kynkäänniemi et al. 2019) reflect generative diversity.

Diffusion schedule. All acceleration methods are compared strictly in the same DDPM(Ho, Jain, and Abbeel 2020) backbone with noisy schedule ($\beta_1 = 2 \times 10^{-4}$, $\beta_T = 0.01$, $T = 1000$), which correspond to discretization of Variance Preserving(VP) SDE(Song et al. 2020), namely, $f(t)$ and $g(t)$ in (5) satisfy $f(t) = \frac{1}{2}\beta(t)$ and $g(t) = \sqrt{\beta(t)}$. In this setting, (5) has a standard Gaussian steady state distribution when $T \rightarrow \infty$, i.e., $p_\infty = \mathcal{N}(\mathbf{0}, \mathbf{I})$. If we want to construct OT accelerated DM with $T' = 100$, we first initialize $\beta_1, \beta_2, \dots, \beta_T$, and then terminate diffusion process at step 100.

End time of sampling process ε . In ref. (Lu et al. 2022), the authors suggest that the diffusion time interval $[0, T = 1000]$ of DDPM is uniformly normalized to $[0, 1]$, and then end time of the sampling process is set to 10^{-3} . In this article, we also follow this choice, therefore $\varepsilon = 1$.

Remark 6 *It is worth mentioning that for the convenience of expression in the experiment, the diffusion termination time of all acceleration models is uniformly denoted as T .*

Evaluation of prior error

In Tab. 1, we list the termination time T required for the benchmark accelerated sampling strategy of DMs. It can be

seen that the existing methods for accelerating solve the approximate inverse probability flow ODE (10) do not pay attention to the forward process, so they all need to complete DMs, resulting in high training cost. However, the early stop strategy saves a lot of training resources by selecting a relatively small T . This is confirmed by the experimental results in section A.3 of (Lyu et al. 2022).

Tab. 1: Quantitative comparison of unconditional generative modeling with other ODE or truncation acceleration methods on one NVIDIA A40. We highlight the best performance in **bold** and the suboptimal with underline. In addition, \downarrow and \uparrow are marked to indicate the desired value direction.

Cifar-10 32×32					
Methods	T	$\mathcal{W}_2(p_T, q_T) \downarrow$	NFE	Sampling Time \downarrow	FID \downarrow
DPM-Solver	1000	223.221	50	0.04	2.65
DEIS	1000	225.326	20	—	2.86
UciPC	1000	230.475	10	—	3.84
ES-DDPM	700	123.732	700	0.91	3.11
ES-DDPM	200	0.0019	200	0.26	5.02
TDPM	99	0.0005	100	0.13	2.97
TDPM+	99	0.0005	100	0.13	2.83
Ours	150	0.0	150	0.11	2.43
Ours	100	0.0	100	<u>0.07</u>	<u>2.00</u>
Ours	50	0.0	50	0.04	1.31
CelebA 64×64					
DPM-Solver	1000	187.286	50	<u>0.19</u>	3.19
DEIS	1000	184.536	50	—	2.95
ES-DDPM	200	0.0012	200	1.05	2.55
TDPM+	49	0.000049	50	0.26	3.28
Ours	150	0.0	150	0.39	2.69
Ours	100	0.0	100	0.25	<u>2.17</u>
Ours	50	0.0	50	0.13	1.92
FFHQ 256×256					
DPM-Solver	1000	250.916	50	2.88	7.39
UciPC	1000	252.964	10	—	6.99
Ours	150	0.0	150	6.89	3.75
Ours	100	0.0	100	4.65	<u>2.84</u>
Ours	50	0.0	50	2.35	2.14

We also calculate the prior error $\mathcal{W}_2(p_T, q_T)$ of different generative modeling methods by using POT(Flamary et al. 2021) in pixel space. For ODE acceleration methods, $q_T = \mathcal{N}(\mathbf{0}, \mathbf{I})$, whereas for truncation strategies that use $\mathcal{G}(\cdot)$ as probability converter, $q_T = \mathcal{G}(\mathcal{N}(\mathbf{0}, \mathbf{I}))$. The results in Tab. 1 suggest that the prior error of DDPM at $T = 1000$ reaches two order of magnitude, which is ignored by ODE acceleration method and can be effectively alleviated by truncation acceleration method. At the same time, Tab. 1 also conveys us an important message that OT can completely eliminate prior errors regardless of the termination time, which echoes the view point of this article. In fact, the geometric variational principle(Gu et al. 2016) theoretically guarantees that the calculated OT must be a one-to-one correspondence between the sampling cell and the target point(As illustrated in Fig. 1 in the Appendix), therefore $\mathcal{W}_2(p_T, q_T) = 0$.

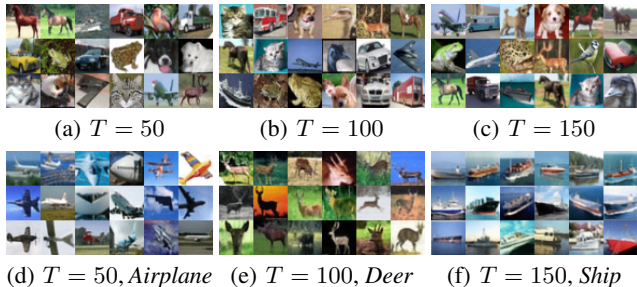


Fig. 1: Generated Cifar-10 32×32 images with OT accelerator. The subgraphs (a), (b), and (c) are unconditional images at different termination times. The subgraphs (d), (e), and (f) display generated images labeled *Airplane* with $T = 50$, *Deer* with $T = 100$, *Ship* with $T = 150$, in turn.

Measurement of sampling efficiency

We use the total running time of sampling process to measure the sampling efficiency. Specifically, we refer to the random noise set as $\{z^i\}_{i=1}^{N_{st}} \stackrel{i.i.d}{\sim} \mathcal{N}(\mathbf{0}, \mathbf{I})$, and the time required to deduce the image x_ε^i from the i -th noise by a certain modeling method is $RunTime(z^i, x_\varepsilon^i)$. Then the average sampling time(second/image) is formulated as

$$Sampling\ Time = \frac{1}{N_{st}} \sum_{i=1}^{N_{st}} RunTime(z^i, x_\varepsilon^i). \quad (18)$$

In this article, we take $N_{st} = 1500$. By reporting the values of (18) for all ODE or truncation acceleration strategies in Tab. 1, it is not difficult to see that our model has the highest sampling efficiency on all three datasets. Although DPM-Solver’s sampling efficiency on Cifar-10 32×32 dataset is basically the same as ours with NFE=50, the very long diffusion time $T = 1000$ leads to their high training cost.

Quantification of generation quality

Apart from the above analysis, we are also interested in the quality of images produced by the OT accelerator. As can be seen from Tab. 1, OT provides a lower FID score compared to the same type of acceleration method on on Cifar-10 32×32, CelebA 64×64 and FFHQ 256 × 256. Beyond that, we find that with the decay of T , the FID value of our method will decrease. In the meantime, we report unconditional generation comparison results in Tab. 2 for more diffusion modeling methods. In general, the proposed model achieves better than or comparable FID, Precision and Recall scores among them. Fig. 1~Fig. 3 visualize the generation effect of our method on three datasets.

Conclusion

This study examines the prior error in DMs, where the termination distribution of the forward process deviates from the initial distribution of the reverse process, and argues that OT is the optimal method for its elimination. We first prove that the DM is essentially a two-stage dynamic OT calculation method, and the quadratic transport cost of the sampling trajectory is also reduced while the score matching loss is optimized. However, the existence of the prior error makes a potential gap stand between the sampling transport and the desired OT. Subsequently, we theoretically find that the probability flow converges exponentially to the gradient

Tab. 2: Quantitative comparison of unconditional generative modeling with other diffusion type methods.

Cifar-10 32×32				
Methods	NFE	FID↓	Precision↑	Recall↑
DDPM	1000	3.31	0.70	0.59
DPM-Solver	20	3.72	0.58	0.53
TDPM	100	2.97	—	0.57
TDPM+	100	2.83	—	0.58
EDM	27	3.73	0.63	0.56
Ours	150	2.43	0.64	0.64
Ours	100	<u>2.00</u>	0.65	<u>0.68</u>
Ours	50	1.31	<u>0.66</u>	0.76
CelebA 64×64				
Methods	NFE	FID↓	Precision↑	Recall↑
DPM-Solver	20	3.13	0.71	0.46
DDIM	100	6.53	0.75	0.42
NCSNv2	2500	10.23	0.85	0.42
Ours	150	2.69	0.73	0.68
Ours	100	<u>2.17</u>	0.77	<u>0.69</u>
Ours	50	1.92	<u>0.79</u>	0.75
FFHQ 256×256				
Methods	NFE	FID↓	Precision↑	Recall↑
Ours	150	3.75	0.75	0.67
Ours	100	<u>2.84</u>	<u>0.76</u>	<u>0.70</u>
Ours	50	2.14	0.77	0.72

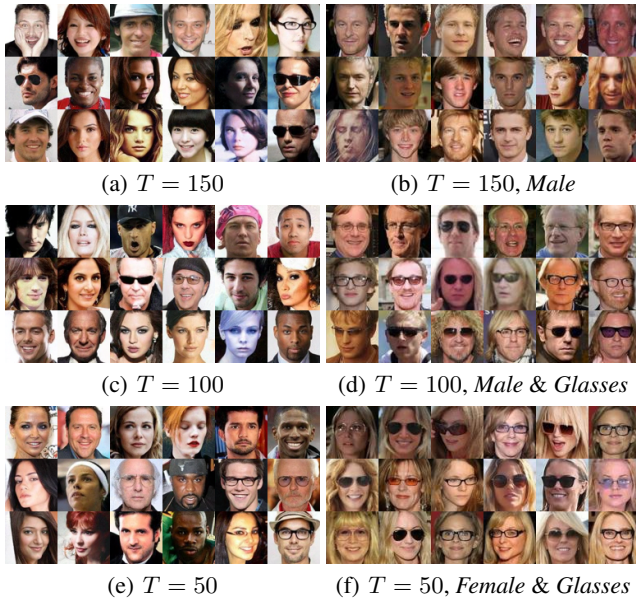


Fig. 2: Generated CelebA 64×64 images with OT sampler. The subgraphs (a), (c) and (e) represent unconditional generated images with different termination times, while the subgraphs (b), (d), and (f) suggest generated images labeled *Male* with $T = 150$, *Male & Glasses* with $T = 100$ and *Female & Glasses* with $T = 50$ in turn.

of solution to the Monge-Ampère equation as the diffusion time increases, which means that OT is not only the most economical but also the most intrinsic prior eliminator compared to other probabilistic converters. Finally, we show that this idea can be naturally applied to accelerated sampling for unconditional and conditional generation. Ob-

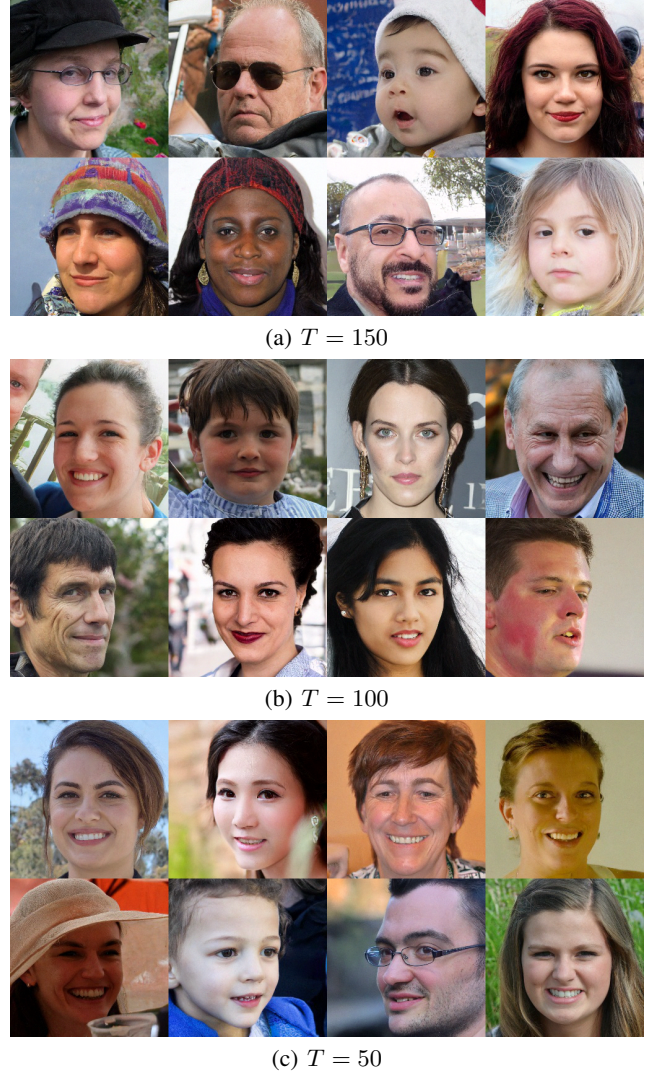


Fig. 3: Generated FFHQ 256×256 images with OT sampler. From the top to the bottom, the three subgraphs (a), (b) and (c) list unconditional generated images with different termination times $T = 50, 100, 150$, respectively.

viously, the progress in this paper strengthens the connection between OT and DMs, but it is also limited to specific cases. The deeper relationship between the two aforementioned in more general settings that are worth digging into in our future work.

References

- Alexandrov, A. D. 2005. *Convex polyhedra*, volume 109. Springer.
- An, D.; Guo, Y.; Lei, N.; Luo, Z.; Yau, S.-T.; and Gu, X. 2020. AE-OT: A New Generative Model Based on Extended Semi-Discrete Optimal Transport. In *Proceedings of the 8th International Conference on Learning Representations*.
- Anderson, B. D. 1982. Reverse-time diffusion equation models. *Stochastic Processes and their Applications*, 12(3): 313–326.
- Arjovsky, M.; Chintala, S.; and Bottou, L. 2017. Wasserstein generative adversarial networks. In *International conference on machine learning*, 214–223. PMLR.
- Benamou, J.-D.; and Brenier, Y. 2000. A computational fluid mechanics solution to the Monge-Kantorovich mass transfer problem. *Numerische Mathematik*, 84(3): 375–393.
- Benton, J.; De Bortoli, V.; Doucet, A.; and Deligiannidis, G. 2023. Linear convergence bounds for diffusion models via stochastic localization. *arXiv preprint arXiv:2308.03686*.
- Brenier, Y. 1991. Polar factorization and monotone rearrangement of vector-valued functions. *Communications on pure and applied mathematics*, 44: 375–417.
- Carrillo, J. A.; McCann, R. J.; and Villani, C. 2006. Contractions in the 2-Wasserstein length space and thermalization of granular media. *Archive for Rational Mechanics and Analysis*, 179: 217–263.
- Chen, S.; and Figalli, A. 2017. Partial W₂, p regularity for optimal transport maps. *Journal of Functional Analysis*, 272(11): 4588–4605.
- Chung, H.; Sim, B.; and Ye, J. C. 2022. Come-Closer-Diffuse-Faster: Accelerating Conditional Diffusion Models for Inverse Problems Through Stochastic Contraction. In *Proceedings of the IEEE/CVF Conference on Computer Vision and Pattern Recognition (CVPR)*, 12413–12422.
- Dhariwal, P.; and Nichol, A. 2021. Diffusion models beat gans on image synthesis. *Advances in neural information processing systems*, 34: 8780–8794.
- Figalli, A. 2010. Regularity properties of optimal maps between nonconvex domains in the plane. *Communications in Partial Differential Equations*, 35: 465–479.
- Flamary, R.; Courty, N.; Gramfort, A.; Alaya, M. Z.; Boisbunon, A.; Chambon, S.; Chapel, L.; Corenflos, A.; Fatras, K.; Fournier, N.; et al. 2021. Pot: Python optimal transport. *Journal of Machine Learning Research*, 22(78): 1–8.
- Franzese, G.; Rossi, S.; Yang, L.; Finamore, A.; Rossi, D.; Filippone, M.; and Michiardi, P. 2023. How much is enough? a study on diffusion times in score-based generative models. *Entropy*, 25(4): 633.
- Gardiner, C. W.; et al. 1985. *Handbook of stochastic methods*, volume 3. Springer Berlin.
- Goodfellow, I.; Pouget-Abadie, J.; Mirza, M.; Xu, B.; Warde-Farley, D.; Ozair, S.; Courville, A.; and Bengio, Y. 2014. Generative adversarial nets. In *Advances in neural information processing systems*, volume 27.
- Gu, X.; Luo, F.; Sun, J.; and Yau, S.-T. 2016. Variational principles for Minkowski type problems, discrete optimal transport, and discrete Monge–Ampère equations. *Asian Journal of Mathematics*, 20(2): 383–398.
- Heusel, M.; Ramsauer, H.; Unterthiner, T.; Nessler, B.; and Hochreiter, S. 2017. GANs trained by a two time-scale update rule converge to a local nash equilibrium. In *Proceedings of the 31st International Conference on Neural Information Processing Systems*, 6629–6640.
- Ho, J.; Jain, A.; and Abbeel, P. 2020. Denoising diffusion probabilistic models. In *Proceedings of the 34th International Conference on Neural Information Processing Systems*, 6840–6851.
- Ho, J.; Salimans, T.; Gritsenko, A.; Chan, W.; Norouzi, M.; and Fleet, D. J. 2022. Video diffusion models. *Advances in Neural Information Processing Systems*, 35: 8633–8646.
- Karras, T.; Aittala, M.; Aila, T.; and Laine, S. 2022. Elucidating the design space of diffusion-based generative models. *Advances in Neural Information Processing Systems*, 35: 26565–26577.
- Khulkov, V.; Ryzhakov, G.; Chertkov, A.; and Oseledets, I. 2022. Understanding DDPM Latent Codes Through Optimal Transport. In *The Eleventh International Conference on Learning Representations*.
- Kingma, D. P.; and Welling, M. 2013. Auto-encoding variational bayes. *arXiv preprint arXiv:1312.6114*.
- Kong, Z.; Ping, W.; Huang, J.; Zhao, K.; and Catanzaro, B. 2020. Diffwave: A versatile diffusion model for audio synthesis. *arXiv preprint arXiv:2009.09761*.
- Krizhevsky, A.; Hinton, G.; et al. 2009. Learning multiple layers of features from tiny images (2009).
- Kwon, D.; Fan, Y.; and Lee, K. 2022. Score-based generative modeling secretly minimizes the wasserstein distance. *Advances in Neural Information Processing Systems*, 35: 20205–20217.
- Kynkäänniemi, T.; Karras, T.; Laine, S.; Lehtinen, J.; and Aila, T. 2019. Improved precision and recall metric for assessing generative models. In *Proceedings of the 33rd International Conference on Neural Information Processing Systems*, 3927–3936.
- Lavenant, H.; and Santambrogio, F. 2022. The flow map of the fokker–planck equation does not provide optimal transport. *Applied Mathematics Letters*, 133: 108225.
- Lee, S.-g.; Kim, H.; Shin, C.; Tan, X.; Liu, C.; Meng, Q.; Qin, T.; Chen, W.; Yoon, S.; and Liu, T.-Y. 2021. Priorgrad: Improving conditional denoising diffusion models with data-dependent adaptive prior. *arXiv preprint arXiv:2106.06406*.
- Lei, N.; Su, K.; Cui, L.; Yau, S.-T.; and Gu, X. D. 2019. A geometric view of optimal transportation and generative model. *Computer Aided Geometric Design*, 68: 1–21.
- Li, S.; Chen, S.; and Li, Q. 2024. A good score does not lead to a good generative model. *arXiv preprint arXiv:2401.04856*.
- Li, Z.; Li, S.; Wang, Z.; Lei, N.; Luo, Z.; and Gu, D. X. 2023. DPM-OT: A New Diffusion Probabilistic Model Based on

- Optimal Transport. In *Proceedings of the IEEE/CVF International Conference on Computer Vision*, 22624–22633.
- Liu, Z.; Luo, P.; Wang, X.; and Tang, X. 2015. Deep learning face attributes in the wild. In *Proceedings of the IEEE international conference on computer vision*, 3730–3738.
- Lu, C.; Zhou, Y.; Bao, F.; Chen, J.; Li, C.; and Zhu, J. 2022. Dpm-solver: A fast ode solver for diffusion probabilistic model sampling in around 10 steps. *Advances in Neural Information Processing Systems*, 35: 5775–5787.
- Luo, Z.; Chen, W.; Lei, N.; Guo, Y.; Zhao, T.; Liu, J.; and Gu, X. 2022. The singularity set of optimal transportation maps. *Computational Mathematics and Mathematical Physics*, 62(8): 1313–1330.
- Lyu, Z.; XU, X.; Yang, C.; Lin, D.; and Dai, B. 2022. Accelerating Diffusion Models via Early Stop of the Diffusion Process. *arXiv:2205.12524*.
- McCann, R. J. 1997. A convexity principle for interacting gases. *Advances in mathematics*, 128(1): 153–179.
- Monge, G. 1781. Mémoire sur la théorie des déblais et des remblais. *Mem. Math. Phys. Acad. Royale Sci.*, 666–704.
- Nichol, A. Q.; and Dhariwal, P. 2021. Improved denoising diffusion probabilistic models. In *International conference on machine learning*, 8162–8171. PMLR.
- Radford, A.; Metz, L.; and Chintala, S. 2015. Unsupervised representation learning with deep convolutional generative adversarial networks. *arXiv preprint arXiv:1511.06434*.
- Rezende, D. J.; Mohamed, S.; and Wierstra, D. 2014. Stochastic backpropagation and approximate inference in deep generative models. In *International conference on machine learning*, 1278–1286. PMLR.
- Risken, H.; and Risken, H. 1996. *Fokker-planck equation*. Springer.
- Russakovsky, O.; Deng, J.; Su, H.; Krause, J.; Satheesh, S.; Ma, S.; Huang, Z.; Karpathy, A.; Khosla, A.; Bernstein, M.; et al. 2015. Imagenet large scale visual recognition challenge. *International journal of computer vision*, 115: 211–252.
- Ruthotto, L.; and Haber, E. 2021. An introduction to deep generative modeling. *GAMM-Mitteilungen*, 44(2): e202100008.
- Sohl-Dickstein, J.; Weiss, E.; Maheswaranathan, N.; and Ganguli, S. 2015. Deep unsupervised learning using nonequilibrium thermodynamics. In *International conference on machine learning*, 2256–2265. PMLR.
- Song, J.; Meng, C.; and Ermon, S. 2020. Denoising diffusion implicit models. *arXiv preprint arXiv:2010.02502*.
- Song, Y.; Dhariwal, P.; Chen, M.; and Sutskever, I. 2023. Consistency models. *arXiv preprint arXiv:2303.01469*.
- Song, Y.; Durkan, C.; Murray, I.; and Ermon, S. 2021. Maximum likelihood training of score-based diffusion models. *Advances in neural information processing systems*, 34: 1415–1428.
- Song, Y.; and Ermon, S. 2019. Generative modeling by estimating gradients of the data distribution. *Advances in neural information processing systems*, 32.
- Song, Y.; and Ermon, S. 2020. Improved techniques for training score-based generative models. *Advances in neural information processing systems*, 33: 12438–12448.
- Song, Y.; Sohl-Dickstein, J.; Kingma, D. P.; Kumar, A.; Ermon, S.; and Poole, B. 2020. Score-based generative modeling through stochastic differential equations. *arXiv preprint arXiv:2011.13456*.
- Tashiro, Y.; Song, J.; Song, Y.; and Ermon, S. 2021. CSDI: Conditional score-based diffusion models for probabilistic time series imputation. *Advances in Neural Information Processing Systems*, 34: 24804–24816.
- Villani, C.; et al. 2009. *Optimal transport: old and new*, volume 338. Springer.
- Vincent, P. 2011. A connection between score matching and denoising autoencoders. *Neural computation*, 23(7): 1661–1674.
- Zhang, P.; Yin, H.; Li, C.; and Xie, X. 2024a. Formulating discrete probability flow through optimal transport. *Advances in Neural Information Processing Systems*, 36.
- Zhang, P.; Yin, H.; Li, C.; and Xie, X. 2024b. Tackling the Singularities at the Endpoints of Time Intervals in Diffusion Models. In *Proceedings of the IEEE/CVF Conference on Computer Vision and Pattern Recognition*, 6945–6954.
- Zhang, Q.; and Chen, Y. 2022. Fast sampling of diffusion models with exponential integrator. *arXiv preprint arXiv:2204.13902*.
- Zhao, W.; Bai, L.; Rao, Y.; Zhou, J.; and Lu, J. 2024. Unipc: A unified predictor-corrector framework for fast sampling of diffusion models. *Advances in Neural Information Processing Systems*, 36.
- Zheng, H.; He, P.; Chen, W.; and Zhou, M. 2022. Truncated Diffusion Probabilistic Models and Diffusion-based Adversarial Auto-Encoders. In *The Eleventh International Conference on Learning Representations*.